CRYSTAL GROWTH & DESIGN

ARTICLE

pubs.acs.org/crystal

Synthesis, Crystal Structures, and Luminescence and Magnetic Properties of 3D Chiral and Achiral Lanthanide Diphosphonates Containing Left- and Right-Handed Helical Chains

Da-Peng Dong,[†] Lei Liu,[†] Zhen-Gang Sun,*[,†] Cheng-Qi Jiao,[†] Zhong-Min Liu,[‡] Chao Li,[†] Yan-Yu Zhu,[†] Kai Chen,[†] and Cheng-Lin Wang[†]

[†]Institute of Chemistry for Functionalized Material, School of Chemistry and Chemical Engineering, Liaoning Normal University, Dalian 116029, P. R. China

[‡]Dalian Institute of Chemical Physics, Chinese Academy of Sciences, Dalian 116023, P. R. China

Supporting Information

ABSTRACT: Using the heptadentate ligand $hedpH_4$ (1-hydroxyethylidenediphosphonic acid) and lanthanide chloride, two isomorphous series of coordination frameworks of the general formula $[NH_4][Ln(hedp)(H_2O)]\cdot H_2O$ (series 1, orthorhombic $P2_12_12_1$, Ln = La (**1**), Ce (**2**), Pr (**3**), Nd (**4**)) and $[NH_4][Ln(hedp)(H_2O)]$ (series 2, orthorhombic *Pnma*, Ln = Sm (**5**), Eu (**6**), Gd (**7**), Tb (**8**), Dy (**9**), Y (**10**), Er (**11**)) have been assembled and characterized with IR, elemental analysis, thermogravimetric analysis, and single-crystal and powder X-ray diffraction methods. In both series, each inorganic chain based on LnO_8 and CPO_3 polyhedra are interconnected through phosphonate ligands to form chiral and achiral 3D open-framework structures with left- and right-handed helical chains. Meanwhile, the two series also exhibit two types of 3D framework structures with similar network topologies. The crystal water molecule plays an important role to induce chiral structure and affects the crystal packing of the molecules with extensive hydrogen bonding. The luminescence properties of compounds **5**, **6**, **8** and **9** and the magnetic property of compound **7** have also been studied.

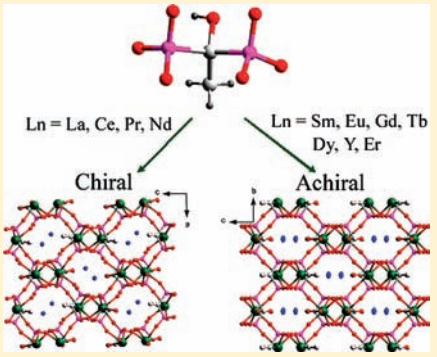

INTRODUCTION

Recently, a considerable amount of the research activity on metal phosphonate chemistry has focused on rational design and synthesis of multifunctional coordination polymers, mainly due to their interesting structures and potential application in the area of catalysis, ion exchange, proton conductivity, intercalation chemistry, photochemistry, and materials chemistry.[1−4] In this realm an encouraging research direction is the synthesis of metal phophonates functionalized with amine, hydroxyl, and carboxylate groups. Introduction of these functional groups may not only result in new structure types of metal phosphonates but also bring interesting properties.

A number of metal phosphonate frameworks with additional functionality have been reported recently.[5−8] Using multifunctional phosphonic acids containing $-NH_2$, $-OH$, and $-COOH$ subfunctional groups and providing many coordination modes as ligands, a series of metal phosphonates with a framework structure have also been isolated in our laboratory.[9] The diphosphonic acids, $H_2O_3P-R-PO_3H_2$ (R = alkyl or aryl group), have been proved to be very useful ligands for the synthesis of metal phosphonates with new structure types in which the organic part plays a controllable spacer role and the two inorganic $-PO_3$ groups chelate with metal ions to form one-, two-, and three-dimensional structures.[10]

In recent years, there has been great interest in the synthesis and properties of chiral metal phosphonates, which are generally obtained either by enantioselective synthesis using enantiopure chiral species or by spontaneous resolution on crystallization without any chiral auxiliary. On the basis of enantiopure phosphonate ligands, a few homochiral metal phosphonates have been prepared.[11] Spontaneous resolution can also be achieved using achiral or racemic ligands as starting materials, which usually results in racemic conglomerates.[12] The phenomenon of spontaneous resolution is unusual in coordination chemistry, and the products are normally a racemic mixture of left- and right-handed helical chains, although the each crystal is a single enantiomer.[13,14] With the aim of exploring new chiral phosphonates with interesting structures and properties, we focus our attention on a flexible and multifunctional bisphosphonic acid ligand ($hedpH_4$, Scheme 1), which has been widely used as a strong chelating agent in the preparation of functional metal diphosphonates, since it can adopt various kinds of coordination modes under different reaction conditions.[15] Moreover, the

Received: July 21, 2011
Revised: September 18, 2011
Published: October 08, 2011

Scheme 1. Structure of 1-Hydroxyethylidenediphosphonic Acid ($hedpH_4$)

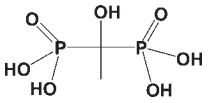

mobility and flexibility of the two phosphonate functions make it easy to coordinate a large number of metal ions with various ionic radii. Among these, many transition metal diphosphonates with interesting magnetic properties have been prepared.[16] Comparatively few reports are available on the magnetic and photoluminescence properties of lanthanide diphosphonates prepared under mild hydrothermal conditions with ammonium as a template.[17] As an extension to our previous work, herein, we report the hydrothermal synthesis, crystal structure, and thermal stability of 11 novel 3D chiral and achiral lanthanide diphosphonates with left- and right-handed helical chains, namely, $[NH_4][Ln(hedp)(H_2O)]\cdot H_2O$ (Ln = La (**1**), Ce (**2**), Pr (**3**), Nd (**4**)) and $[NH_4][Ln(hedp)(H_2O)]$ (Ln = Sm (**5**), Eu (**6**), Gd (**7**), Tb (**8**), Dy (**9**), Y (**10**), Er (**11**)). The luminescence properties of compounds **5**, **6**, **8**, and **9** and the magnetic property of compound **7** have also been studied.

EXPERIMENTAL SECTION

Materials and Methods. 1-Hydroxyethylidenediphosphonic acid solution was obtained from Taihe Chemical Factory as a water treatment agent (50.0 wt %) and used as received. The lanthanide(III) chlorides were prepared by dissolving corresponding lanthanide oxides (General Research Institute for Nonferrous Metals, 99.99%) in hydrochloric acid followed by recrystallization and drying. All other chemicals were used as obtained without further purification. C, H, and N were determined byusing a PE-2400 elemental analyzer. La, Ce, Pr, Nd, Sm, Eu, Gd, Tb, Dy, Y, Er, and P were determined using an inductively coupled plasma (ICP) atomic absorption spectrometer. IR spectra were recorded on a Bruker AXS TENSOR-27 FT-IR spectrometer with KBr pellets in the range 4000−400 cm^{-1}. X-ray powder diffraction data was collected on a Bruker AXS D8 Advance diffractometer using Cu Kα radiation (λ = 1.5418 Å) in the 2θ range of 5−60° with a step size of 0.02° and a scanning rate of 3°/min. TG analyses were performed on a Perkin-Elmer Pyris Diamond TG-DTA thermal analyses system in static air with a heating rate of 10 K min^{-1} from 50 to 1000 °C. The luminescence spectra were reported on a JASCO FP-6500 spectrofluorimeter (solid). Variable-temperature magnetic susceptibility data were obtained on a SQUID magnetometer (Quantum Design, MPMS-7) in the temperature range of 2−300 K with an applied field of 1000 Oe.

Synthesis of $[NH_4][Ln(hedp)(H_2O)]\cdot H_2O$ (Ln = La (1), Ce (2), Pr (3), Nd (4)). The methods used for the syntheses of compounds **1**−**4** are similar. A mixture of $LnCl_3\cdot 6H_2O$ (0.09 g, 0.25 mmol), $hedpH_4$ solution (1 mL, 2.5 mmol), and $H_2C_2O_4\cdot 2H_2O$ (0.12 g, 1 mmol) in 10 mL of deionized water, adjusted to pH ≈ 7 with an aqueous solution of NH_3 while stirring, was sealed in a 20 mL Teflon-lined stainless steel autoclave and then heated at 160 °C for 78 h. After the mixture was cooled slowly to room temperature, suitable crystals of **1**−**4** were obtained. For **1**, yield: 61.2% based on La. Anal. Calcd for $C_2H_{12}NO_9P_2La$: C, 6.08; H, 3.06; N, 3.54; P, 15.70; La, 35.17. Found: C, 6.11; H, 3.10; N, 3.49; P, 15.68; La, 35.21. IR (KBr, cm^{-1}): 3573 (w), 3345 (m), 3151 (s), 1620 (w), 1452 (m), 1081 (s), 997 (w), 946 (w), 811 (w), 661 (w), 576 (w), 459 (w). For **2**, yield: 64.6% based on Ce. Anal. Calcd for $C_2H_{12}NO_9P_2Ce$: C, 6.06; H, 3.05; N, 3.53; P, 15.65; Ce, 35.37. Found: C, 6.10; H, 3.01; N, 3.56; P, 15.62; Ce, 35.32. IR (KBr, cm^{-1}): 3579 (w), 3350 (m), 3190 (s), 1654 (w), 1434 (m), 1091 (s), 995 (w), 948 (w), 813 (w), 671 (w), 567 (w), 464 (w). For **3**, yield: 65.6% based on Pr. Anal. Calcd for $C_2H_{12}NO_9P_2Pr$: C, 6.05; H, 3.02; N, 3.53; P, 15.62; Pr, 35.50. Found: C, 6.07; H, 3.07; N, 3.50; P, 15.65; Pr, 35.46. IR (KBr, cm^{-1}): 3571 (w), 3325 (m), 3184 (s), 1635 (w), 1448 (m), 1091 (s), 1009 (w), 956 (w), 819 (w), 665 (w), 574 (w), 476 (w). For **4**, yield: 60.9% based on Nd. Anal. Calcd for $C_2H_{12}NO_9P_2Nd$: C, 6.00; H, 3.00; N, 3.50; P, 15.49; Nd, 36.03. Found: C, 6.04; H, 3.05; N, 3.54; P, 15.55; Nd, 36.06. IR (KBr, cm^{-1}): 3574 (w), 3367 (m), 3174 (s), 1623 (w), 1434 (m), 1099 (s), 1000 (w), 964 (w), 827 (w), 671 (w), 580 (w), 470 (w).

Synthesis of $[NH_4][Ln(hedp)(H_2O)]$ (Ln = Sm (5), Eu (6), Gd (7), Tb (8), Dy (9), Y (10), Er (11)). The methods used for the syntheses of compounds **5**−**11** are similar. A mixture of $LnCl_3\cdot 6H_2O$ (0.09 g, 0.25 mmol), $hedpH_4$ solution (1 mL, 2.5 mmol), and $H_2C_2O_4\cdot 2H_2O$ (0.12 g, 1 mmol) in 10 mL of deionized water, adjusted to pH ≈ 7 with an aqueous solution of NH_3 while stirring, was sealed in a 20 mL Teflon-lined stainless steel autoclave and then heated at 160 °C for 78 h. After the mixture was cooled slowly to room temperature, suitable crystals of **5**−**11** were obtained. For **5**, yield: 62.3% based on Sm. Anal. Calcd for $C_2H_7NO_8P_2Sm$: C, 6.23; H, 1.83; N, 3.63; P, 16.09; Sm, 39.02. Found: C, 6.25; H, 1.86; N, 3.59; P, 16.14; Sm, 39.07. IR (KBr, cm^{-1}): 3494 (m), 3197 (s), 1662 (w), 1440 (m), 1099 (s), 1008 (w), 962 (w), 835 (w), 671 (w), 567 (w), 484 (w). For **6**, yield: 63.6% based on Eu. Anal. Calcd for $C_2H_7NO_8P_2Eu$: C, 6.20; H, 1.82; N, 3.62; P, 16.02; Eu, 39.27. Found: C, 6.18; H, 1.87; N, 3.57; P, 16.08; Eu, 39.31. IR (KBr, cm^{-1}): 3498 (w), 3197 (s), 1645 (w), 1427 (m), 1110 (s), 1014 (w), 835 (w), 665 (w), 568 (w), 487 (w). For **7**, yield: 62.7% based on Gd. Anal. Calcd for $C_2H_7NO_8P_2Gd$: C, 6.12; H, 1.80; N, 3.57; P, 15.81; Gd, 40.09. Found: C, 6.14; H, 1.76; N, 3.52; P, 15.78; Gd, 40.13. IR (KBr, cm^{-1}): 3429 (w), 3224 (s), 1654 (w), 1434 (m), 1118 (s), 1008 (w), 838 (w), 671 (w), 574 (w), 484 (w). For **8**, yield: 61.8% based on Tb. Anal. Calcd for $C_2H_7NO_8P_2Tb$: C, 6.09; H, 1.79; N, 3.55; P, 15.74; Tb, 40.34. Found: C, 6.14; H, 1.84; N, 3.51; P, 15.70; Tb, 40.38. IR (KBr, cm^{-1}): 3494 (w), 3203 (s), 1654 (w), 1429 (m), 1110 (s), 1000 (m), 846 (w), 667 (w), 578 (w), 479 (w). For **9**, yield: 61.8% based on Dy. Anal. Calcd for $C_2H_7NO_8P_2Dy$: C, 6.04; H, 1.77; N, 3.52; P, 15.60; Dy, 40.88. Found: C, 6.09; H, 1.81; N, 3.47; P, 15.63; Dy, 40.82. IR (KBr, cm^{-1}): 3498 (w), 3199 (s), 1652 (w), 1434 (m), 1110 (s), 1014 (m), 844 (w), 665(w), 576 (w), 487 (w). For **10**, yield: 63.5% based on Y. Anal. Calcd for $C_2H_7NO_8P_2Y$: C, 7.41; H, 2.18; N, 4.32 P, 19.14; Y, 58.32. Found: C, 7.46; H, 2.15; N, 4.36; P, 19.18; Y, 58.26. IR (KBr, cm^{-1}): 3468 (w), 3172 (s), 1635 (w), 1440(m), 1084 (s), 1014 (m), 844 (w), 671(w), 567 (w), 489 (w). For **11**, yield: 62.7% based on Er. Anal. Calcd for $C_2H_7NO_8P_2Er$: C, 5.97; H, 1.75; N, 3.48 P, 15.41; Er, 41.58. Found: C, 6.02; H, 1.79; N, 3.53; P, 15.46; Er, 41.53. IR (KBr, cm^{-1}): 3494 (w), 3190 (m), 1662 (w), 1440 (m), 1099 (s), 1008 (w), 837 (w), 676 (w), 561 (w), 495 (w).

Crystallographic Studies. Data collection for compounds **1**−**11** was performed on a Bruker AXS Smart APEX II CCD X-diffractometer equipped with graphite-monochromated Mo Kα radiation (λ = 0.71073 Å) at 293 ± 2K. An empirical absorption correction was applied using the SADABS program. Structures were solved by direct methods and refined by full matrix least-squares on F^2 using the programs SHELXS-97. All non-hydrogen atoms were refined anisotropically. Hydrogen atoms except those for water molecules were generated geometrically with fixed isotropic thermal parameters and included in the structure factor calculations. Hydrogen atoms for water molecules were not included in the refinement. Details of crystallographic data are given in Table 1 for compounds **1**−**4** and Table 2 for compounds **5**−**11**. Hydrogen-bonding geometric data in compounds **2** and **6** listed in Table 3.

Table 1. Crystal Data and Structure Refinement for Compounds 1−4

compounds	1	2	3	4
empirical formula	$C_2H_{12}NO_9P_2La$	$C_2H_{12}NO_9P_2Ce$	$C_2H_{12}NO_9P_2Pr$	$C_2H_{12}NO_9P_2Nd$
M_r	394.98	396.19	396.98	400.31
cryst syst	orthorhombic	orthorhombic	orthorhombic	orthorhombic
space group	$P2(1)2(1)2(1)$	$P2(1)2(1)2(1)$	$P2(1)2(1)2(1)$	$P2(1)2(1)2(1)$
a/Å	8.7115(10)	8.6912(11)	8.6544(16)	8.649(2)
b/Å	10.4316(13)	10.3935(13)	10.3809(18)	10.323(3)
c/Å	10.8838(13)	10.8180(13)	10.7646(19)	10.738(3)
V/Å^3	989.1(2)	977.2(2)	967.1(3)	958.8(4)
Z	4	4	4	4
D_c/g cm^{-3}	2.653	2.693	2.726	2.773
goodness-of-fit on F^2	1.034	1.032	1.001	1.023
R_1 $[I > 2\sigma(I)]$ [a]	0.0345	0.0318	0.0436	0.0386
wR_2 $[I > 2\sigma(I)]$[a]	0.0667	0.0570	0.0660	0.0707
R_1 (all data) [a]	0.0432	0.0420	0.0695	0.0517
wR_2 (all data) [a]	0.0702	0.0600	0.0732	0.0758

[a] $R_1 = \Sigma(||F_0| - |F_C||)/\Sigma F_0|$, $wR_2 = [\Sigma w(|F_0| - |F_C|)^2/\Sigma wF_0^2]^{1/2}$.

Table 2. Crystal Data and Structure Refinement for Compounds 5−11

compounds	5	6	7	8	9	10	11
empirical formula	$C_2H_7NO_8P_2Sm$	$C_2H_7NO_8P_2Eu$	$C_2H_7NO_8P_2Gd$	$C_2H_7NO_8P_2Tb$	$C_2H_7NO_8P_2Dy$	$C_2H_7NO_8P_2Y$	$C_2H_7NO_8P_2Er$
M_r	385.38	386.99	392.28	393.95	397.53	323.94	402.29
cryst syst	orthorhombic	orthorhombic	orthorhombic	orthorhombic	orthorhombic	orthorhombic	orthorhombic
space group	*Pnma*	*Pnma*	*Pnma*	*Pnma*	*Pnma*	*Pnma*	*Pnma*
a/Å	10.3848(13)	10.3513(14)	10.324(2)	10.297(2)	10.2565(14)	10.2241(19)	10.196(3)
b/Å	8.3420(10)	8.3264(11)	8.3130(17)	8.3034(17)	8.2892(12)	8.2756(16)	8.260(2)
c/Å	10.5774(13)	10.5584(14)	10.534(2)	10.500(2)	10.4595(15)	10.434(2)	10.406(3)
V/Å^3	916.32(19)	910.0(2)	904.1(3)	897.7(3)	889.2(2)	882.8(3)	876.4(4)
Z	4	4	4	4	4	4	4
D_c/g cm^{-3}	2.793	2.825	2.882	2.915	2.969	2.437	3.049
goodness-of-fit on F^2	1.072	1.045	1.034	1.038	1.040	1.013	1.063
R_1 $[I > 2\sigma(I)]$ [a]	0.0567	0.0521	0.0549	0.0492	0.0473	0.0690	0.0464
wR_2 $[I > 2\sigma(I)]$[a]	0.1508	0.1263	0.1138	0.1031	0.1146	0.1773	0.0875
R_1 (all data) [a]	0.0617	0.0624	0.0770	0.0598	0.0562	0.0790	0.0640
wR_2 (all data) [a]	0.1540	0.1318	0.1222	0.1077	0.1190	0.1832	0.0929

[a] $R_1 = \Sigma(||F_0| - |F_C||)/\Sigma|F_0|$, $wR_2 = [\Sigma w(|F_0| - |F_C|)^2/\Sigma wF_0^2]^{1/2}$.

RESULTS AND DISCUSSION

Syntheses. Using the heptadentate ligand $hedpH_4$ (1-hydroxyethylidenediphosphonic acid) and lanthanide chloride, 11 novel 3D chiral and achiral lanthanide diphosphonates with left- and right-hand helical chains have been synthesized under hydrothermal conditions. The best crystallinity of the reaction product was observed in the reactions containing Ln^{3+}, $hedpH_4$, and $H_2C_2O_4 \cdot 2H_2O$ in a molar ratio of 1:10:4. Interestingly, the oxalic acid plays a key role in formation of compounds **1**−**11**. We tried to obtain them without the presence of oxalic acid, but no good samples for X-ray diffraction study were obtained. Even though the dicarboxylic acid was not included in the final product, its inclusion in the reactive mixture is crucial to isolate good-quality single crystals of all the compounds. $NH_3 \cdot H_2O$ was employed as a template and to adjust the pH of the reaction mixture. The ammonium template is critical to form these crystalline materials. To further study their roles in crystal formation, an analogous template 1,4-butanediamine can be used in the synthesis of such materials; however, we gained a series of 1D infinite chains with general formula $[NH_3(CH_2)_4NH_3]Ln[hedpH][hedpH_2]$.[17b,18] Other amines have been used to be a template in the reaction mixture, but we failed to collect suitable single crystals for X-ray diffraction. We also attempted to determine if the ammonium ions can be replaced by other templates. Fortunately, a series of similar 3D open-framework structures with general formula $Na_4[Ln_2(hedp)_2(H_2O)_2] \cdot nH_2O$[17a] was abtained when NaOH was added to the reaction mixture.

Crystal Structures of 1−4. Compounds **1**−**4** are isomorphous; hence, only the structure of **2** will be discussed in detail as a representation. X-ray single-crystal diffraction reveals that compound **2** crystallizes in orthorhombic chiral space group $P2_12_12_1$ (No. 19) with a Flack parameter of 0.01(3). As shown in Figure 1a, each asymmetric unit contains one Ce(III) atom, one $hedp^{4-}$ ligand, one coordinated water molecule, one lattice water

dx.doi.org/10.1021/cg2009368 |*Cryst. Growth Des.* 2011, 11, 5346–5354

Table 3. Hydrogen-Bonding Geometric Data (Å, deg) in Compounds 2 and 6[a]

D−H···A	d(D−H)	d(H···A)	d(D···A)	<(DHA)
compound **2** (Ce)				
O(7)−H(7A)···O(5)^{v}	0.85	1.97	2.777(7)	157.5
O(8)−H(8A)···O(2)^{vii}	0.85	2.00	2.749(6)	146.8
O(8)−H(8B)···O(1W)^{vi}	0.85	1.95	2.703(7)	146.8
O(1W)−H(1WA)···O(1)	0.85	2.26	2.823(8)	123.5
O(1W)−H(1WA)···O(5)^{iii}	0.85	2.36	3.011(7)	134.2
N(1)−H(1D)···O(2)^{i}	0.90	2.24	2.836(8)	123.4
N(1)−H(1A)···O(1W)^{iv}	0.90	1.99	2.879(9)	169.6
N(1)−H(1B)···O(6)^{ii}	0.90	2.29	2.845(8)	119.3
N(1)−H(1B)···O(4)^{ii}	0.90	2.34	3.101(8)	142.4
N(1)−H(1C)···O(7)^{iii}	0.90	2.14	2.991(7)	158.6
compound **6** (Eu)				
O(4)−H(4A)···O(3)^{v}	0.85	2.39	3.185(13)	156.7
O(5)−H(5A)···N(1)	0.85	2.33	2.89(2)	124.0
N(1)−H(1D)···O(5)	0.90	2.27	2.89(2)	126.0
N(1)−H(1D)···O(2)^{i}	0.90	2.36	3.059(19)	135.3
N(1)−H(1D)···O(2)^{ii}	0.90	2.36	3.059(19)	135.3
N(1)−H(1A)···O(4)^{iii}	0.90	2.32	2.95(2)	127.2
N(1)−H(1B)···O(3)^{iv}	0.90	2.58	3.322(15)	140.5

[a] Symmetry transformations used to generate equivalent atoms. For **2**: i $-x+3/2, -y+1, z-1/2$; ii $x+1/2, -y+1/2, -z+1$; iii $-x+1, y-1/2, -z+3/2$; iv $x-1/2, -y+1/2, -z+1$; v $x+1/2, -y+3/2, -z+2$; vi $x-1/2, -y+3/2, -z+2$; vii $-x+1, y+1/2, -z+3/2$. For **6**: i $-x+3/2, y+1/2, z+1/2$; ii $-x+3/2, -y, z+1/2$; iii $x, y, z+1$; iv $-x+1, y+1/2, -z+1$; v $-x+1, y+1/2, -z$.

molecule, and one NH_4^+ cation. The Ce atoms are eight coordinated by six phosphonate oxygen atoms (O2, O5, O4A, O3B, O1C, O6C) from four separate $hedp^{4-}$ ligands, one hydroxyl oxygen atom (O7) from one $hedp^{4-}$ ligand, and one oxygen atom (O8) from one coordinated water molecule. The values of the Ce−O bond lengths are in the range of 2.396(5)−2.755(4) Å, which are comparable to those reported for other Ce(III) phosphonate compounds.[19] Each L^{3-} anion acts as a heptadentate ligand and connects four Ce(III) atoms via all its phosphonate oxygen atoms and hydroxyl oxygen atoms.

In compound **2**, each CeO_8 polyhedron is linked to each other through CPO_3 tetrahedra and thereby to form an infinite chain along the *b* axis. Such infinite chains are linked to form a three-dimensional framework structure via CPO_3 tetrahedra (Figure 2). The result of connections in this manner is formation of two types of 16-atom channels with dimensions of 9.5 Å × 8.5 Å and 10 Å × 9 Å along the crystallographic *a* and *b* axis, respectively (Figure 1b and 1c). The effective free volume of **2** is 123.9 Å^3 (12.7% of the unit cell volume), as calculated by PLATON. The two types of channels have windows made up of 16 atoms, which consist of four Ce, four P, and eight O atoms with the sequences −Ce−O−P−O−Ce−O−P−O−Ce−O−P−O−Ce−O−P−O− and the lattice water molecules and charge−compensating protonated NH_4^+ ions as templates being located inside this channel with extensive hydrogen-bonding interactions (Figure 1d). The N···O distances are 2.836(8), 3.101(8), 2.845(8), 2.991(7), and 2.879(9) Å for N(1)−H(1D)···O(2)^{i}, N(1)−H(1B)···O(4)^{ii}, N(1)−H(1B)···O(6)^{ii}, N(1)−H(1C)···O(7)^{iii}, and N(1)−H(1A)···O(1W)^{iv} (symmetry code: (i) $-x+3/2, -y+1, z-1/2$; (ii) $x+1/2, -y+1/2, -z+1$; (iii) $-x+1, y-1/2, -z+3/2$; (iv) $x-1/2, -y+1/2, -z+1$), respectively. The hydroxyl oxygen atom (O7) also forms a hydrogen bond with a phosphonate oxygen atom (O5): O(7)−H(7A)···O(5)^{v} (symmetry code (v) $x+1/2, -y+3/2, -z+2$) and the bond distances is 2.777(7) Å. Meanwhile, lattice water and coordination water also form a hydrogen bond with a distance of 2.703(7) Å for O(8)−H(8B)···O(1W)^{vi} (symmetry code (vi) $x+1/2, -y+3/2, -z+2$). Another important hydrogen bonding interaction is between the lattice water (O1W)/coordination water (O8) and coordinated phosphonate oxygen atoms (O1, O2, O5): O(1W)−H(1WA)···O(1), O(1W)−H(1WA)···O(5)^{iii}, and O(8)−H(8A)···O(2)^{vii} (symmetry code for (vii) $-x+1, y+1/2, -z+3/2$), and the bond lengths are 2.823(8), 3.011(7), and 2.749(6) Å, respectively. These strong hydrogen bonds enhance the stability of the network and affect the crystal packing of the molecules.

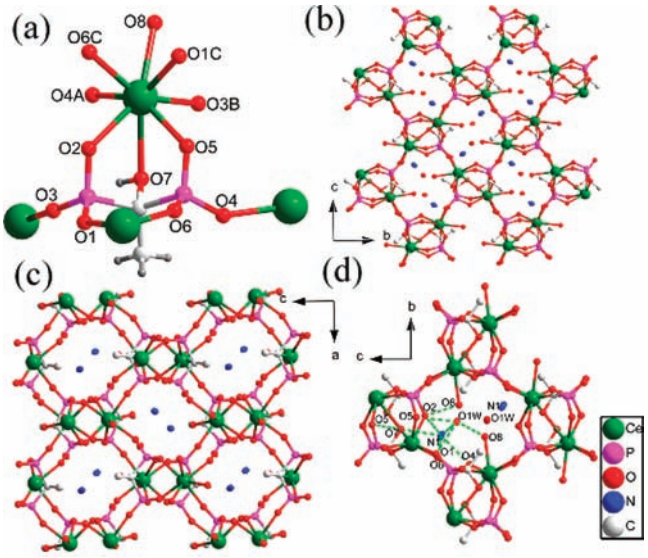

Figure 1. (a) Fragment of the structure in compound **2** with partial atomic labeling scheme. (b) Ball-and-stick view of the framework for compound **2** along the *a* axis. (c) Ball-and-stick view of the framework for compound **2** along the *b* axis. (d) Perspective view of the 1D channels structure in compound **2** showing the hydrogen bonds along the *a* axis. All H atoms are omitted for clarity.

Interestingly, a notable feature for compound **2** is the presence of left- and right-handed helical chains in the structure along the *b* axis, which are connected through Ce−O−P−O−Ce linkages (Figure 3). By comparing with other series of compounds, the chirality of compound **2** may originate from the extensive hydrogen-bonding interactions, such as crystal water molecule, which change the molecular steric orientation of protonated NH_4^+, and induce NH_4^+ as templates to form the chiral configuration (Figure 1c). The interactions also influence the cerium coordination geometry, which exhibits a chiral configuration, and induce the distorted asymmetric framework, which transfers the chirality to three dimensions and generates the spontaneous resolution.

Crystal Structures of 5−11. Compounds **5**−**11** are also isomorphous; hence, only the structure of **6** will be discussed in detail as a representation. X-ray single-crystal diffraction reveals that compound **6** crystallizes in orthorhombic achiral space group *Pnma* (No. 62). As shown in Figure 4a, each

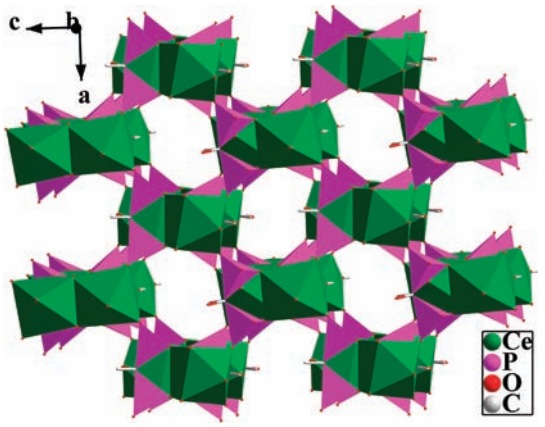

Figure 2. Polyhedral views of 3D framework structures of compound **2** along the *b* axis showing channels (10.0 Å × 9.0 Å). All H are omitted for clarity.

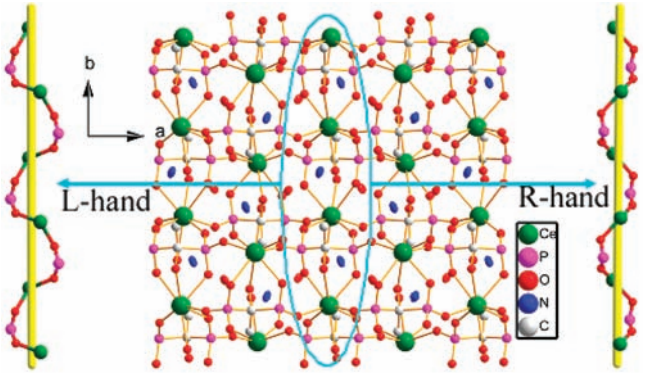

Figure 3. View of the left- and right-handed helical chains of compound **2** along the *b* axis.

asymmetric unit contains one-half Eu(III) atom, one-half $hedp^{4-}$ ligand, one-half coordinated water molecule, and one-half NH_4^+ cation. The Eu atoms are eight coordinated by six phosphonate oxygen atoms (O3, O3C, O1A, O1B, O2D, O2E) from four separate $hedp^{4-}$ ligands, one hydroxyl oxygen atom (O4) from one $hedp^{4-}$ ligand, and one oxygen atom (O5) from one coordinated water molecule. The values of the Eu−O bond lengths are in the range of 2.301(10)−2.685(14) Å, which are comparable to those reported for other Eu(III) phosphonate compounds.[20] Each L^{3-} anion acts as a heptadentate ligand and connects four Eu(III) atoms via all its phosphonate oxygen atoms and hydroxyl oxygen atoms.

For compound **6**, it has a similar 3D framework structure with compound **2** except they are different in the packing direction and hydrogen-bonding mode. Each EuO_8 polyhedron is linked to each other through CPO_3 tetrahedra and thereby to form an infinite chain along the *a* axis. Such infinite chains are linked to form a 3D framework structure via CPO_3 tetrahedra (Figure 5). The result of connections in this manner is formation of two types of 16-atom channels with dimensions of 9.4 Å × 8.3 Å and 9.4 Å × 8.9 Å along the crystallographic *a* and *b* axis, respectively (Figure 4b and 4c). The effective free volume of **6** is 39.0 $Å^3$ (4.3% of the unit cell volume) less than compound **2**, as calculated by PLATON. The two types of channels have windows made up of 16 atoms, which consist of four Eu, four P, and eight O atoms

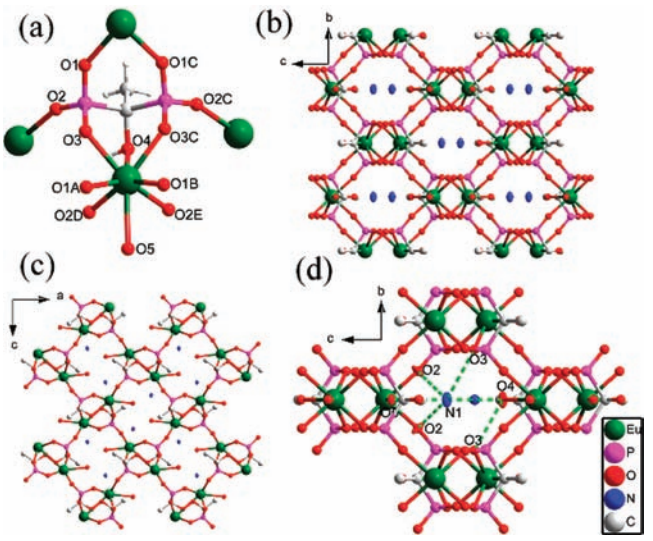

Figure 4. (a) Fragment of the structure in compound **6** with partial atomic labeling scheme. (b) Ball-and-stick view of the framework for compound **6** along the *a* axis. (c) Ball-and-stick view of the framework for compound **6** along the *b* axis. (d) Perspective view of the 1D channels structure in compound **6** showing the hydrogen bonds along the *a* axis. All H atoms are omitted for clarity.

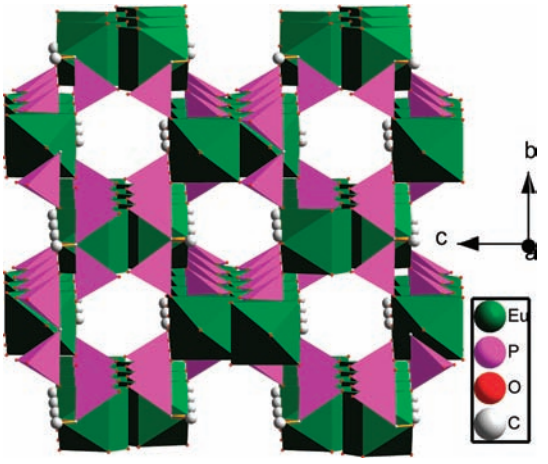

Figure 5. Polyhedral views of 3D framework structures of compound **6** along the *a* axis showing channels (9.4 Å × 8.3 Å). All H are omitted for clarity.

with the sequences −Eu−O−P−O−Eu−O−P−O−Eu−O−P−O−Eu−O−P−O− and the charge-compensating protonated NH_4^+ ions as templates being located inside this channel with extensive hydrogen−bonding interactions (Figure 4d). The N···O distances are 3.059(19), 3.059(19), 2.95(2), and 3.322(15) Å for N(1)−H(1D)···O(2)^{i}, N(1)−H(1D)···O(2)^{ii}, N(1)−H(1A)···O(4)^{iii}, and N(1)−H(1B)···O(3)^{iv} (symmetry code (i) $-x+3/2, y+1/2, z+1/2$; (ii) $-x+3/2, -y, z+1/2$; (iii) $x, y, z+1$; (iv) $-x+1, y+1/2, -z+1$), respectively. The hydroxyl oxygen atom (O4) also forms a hydrogen bond with a phosphonate oxygen atom (O3): O(4)−H(4A)···O(3)^{v} (symmetry code (v) $-x+1, y+1/2, -z$), and the bond distance is 3.185(13) Å. Another important hydrogen bonding is between the coordination water (O5) and protonated NH_4^+ ions (N1): O(5)−H(5A)···N(1) and N(1)−H(1D)···O(5), and the

dx.doi.org/10.1021/cg2009368 |*Cryst. Growth Des.* 2011, 11, 5346–5354

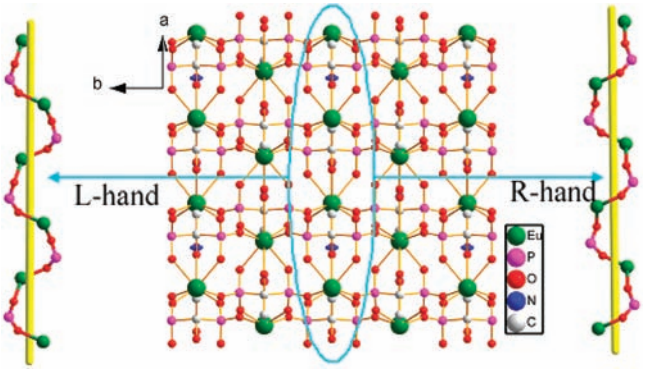

Figure 6. View of the left- and right-handed helical chains of compound **6** along the *a* axis.

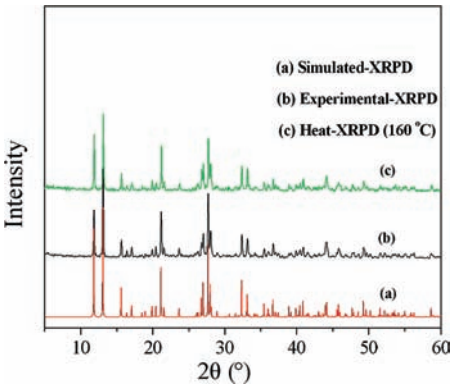

Figure 7. Experimental and heated (160 °C) X-ray powder diffraction diagram of compound **2** compared to the calculated one.

two bond lengths are 2.89(2) Å. These strong hydrogen bonds enhance the stability of the network and affect the crystal packing of the molecules.

In contrast to compound **2**, the crystal structure of compound **6** is still containing left- and right-handed helical chains along the *a* axis, which are connected through Eu−O−P−O−Eu linkages (Figure 6). However, compound **6** has an achiral 3D framework structure, despite the fact that they have similar 3D network topologies, since the compound does not contain a crystal water molecule; as a result, the symmetric NH_4^+ is a templates to form some parallel channels and lead to an achiral configuration (Figure 4b). Thus, the steric orientation of protonated NH_4^+ is very important, which was adjusted by a crystal water molecule that induces different structural packing, steric orientation, and symmetry breaking. The phenomenon of the crystal water molecule to induce NH_4^+ as a template to form a chiral configuration by extensive hydrogen-bonding interactions is still rare to this day. Another reason may be related to the ionic radii of different lanthanide ions, because lanthanide(III) ions change significantly in size across the periodic table, with ionic radii that range from 1.160 (La^{III}) to 0.977 Å (Lu^{III}) for eight-coordinate ions.[21] The large ionic radii for compounds **1**−**4** may have some influence on the chiral configuration.

IR Spectroscopy. IR spectra for compounds **1**−**11** are recorded in the region 4000−400 cm^{-1}. The IR spectra of the 11 compounds have many similar features corresponding to the common groups; thus, only the spectrum of compound **2** will be discussed (Figure S1, Supporting Information). The broad band in the 3579−3190 cm^{-1} region corresponds to the O−H stretching vibrations of hydroxyl groups (including water molecules and 1-hydroxyethylidenediphosphonic acid) and the vibrations of N−H stretching of NH_4^+ cations. A weak band at 1620 cm^{-1} is attributed to the H−O−H bending vibration of water molecules. The medium absorption band at 1434 cm^{-1} is due to the bending vibration of C−H. The set of bands between 1200 and 900 cm^{-1} is due to stretching vibrations of the tetrahedral CPO_3 groups, as expected.[22] Additional weak bands at low energy are found. These bands are probably due to bending vibrations of the tetrahedral CPO_3 groups.

Thermal Analysis. Thermal gravimetric analyses (TGA) are conducted to examine the stabilities of these compounds. The TGA curves of compounds **1**−**4** are similar, with three main continuous weight losses. Herein, we use compound **2** as an example to illuminate the weight losses in detail. As shown in Figure S2, Supporting Information, the first step started at 50 °C and was completed at 300 °C, corresponding to release of one lattice water molecule and one protonated NH_4^+ ion. The observed weight loss of 8.8% is close to the calculated value (9.1%). The second step occurred above 300 °C, during which the compound is partially decomposed. The third step between 360 and 900 °C can be attributed to further decomposition of phosphonate units. The total weight loss of 22.8% is close to the calculated value (23.0%) if the final product is assumed to be a mixture of $Ce(PO_3)_3$ and $CePO_4$ in a molar ratio 1:1. The TGA curves of compounds **5**−**11** are also similar; compound **6** was used as an example (Figure S3, Supporting Information). It exhibits three main continuous weight losses. The first step, in the temperature range 50−140 °C, is due to removal of one protonated NH_4^+ ion. The observed weight loss of 5.2% is close to the calculated value (4.7%). The second step occurred above 140 °C, during which the compound is partially decomposed. The third step covers from 370 to 800 °C, corresponding to further decomposition of the organic groups. The final residual of the thermal process is the mixture of $Eu(PO_3)_3$ and $EuPO_4$ in a molar ratio of 1:1. The total weight loss of 18.0% is close to the calculated value (17.8%). Considering the thermal stability of the compounds, X-ray powder diffraction studies were performed for the as-synthesized compound **2** and the samples calcined at 160, 180, 200, 220, 250, and 280 °C for 2 h, respectively (Figure S4, Supporting Information). The XRD patterns for the calcined samples fit well with that of the as-synthesized sample, indicating that the structure of these compounds can be kept after the dehydration process (Figure 7). Attempts to obtain precise structures from the dehydrated crystals were unsuccessful, which was attributed to the poor crystal quality after water molecules were removed from the lattice.

Photoluminescence Properties. The solide-state luminescence properties of compounds **5**, **6**, **8**, and **9** were investigated at room temperature. The emission spectrum of compound **5** at the excited wavelength of 406 nm is shown in Figure 8. There are three characteristic bands, which are attributed to $^4G_{5/2} \rightarrow {}^6H_J$ (J = 5/2, 7/2, 9/2), $^4G_{5/2} \rightarrow {}^6H_{5/2}$ (563 nm), $^4G_{5/2} \rightarrow {}^6H_{7/2}$ (600 nm), and $^4G_{5/2} \rightarrow {}^6H_{9/2}$ (646 nm) transitions.[9a] Under excitation of 395 nm, compound **6** displays strong red luminescence properties characteristic of the Eu(III) ion (Figure 9). The emission bands at 595, 614, 652, and 700 nm are attributed to $^5D_0 \rightarrow {}^7F_J$ (J = 1−4) transitions.[23] Two stronger peaks are attributed to $^5D_0 \rightarrow {}^7F_1$ (595 nm) and $^5D_0 \rightarrow {}^7F_2$ (614 nm), and the two weaker peaks belong to the transitions of $^5D_0 \rightarrow {}^7F_3$ (652 nm) and $^5D_0 \rightarrow {}^7F_4$ (700 nm). The $^5D_0 \rightarrow {}^7F_1$ transition

dx.doi.org/10.1021/cg2009368 |*Cryst. Growth Des.* 2011, 11, 5346–5354

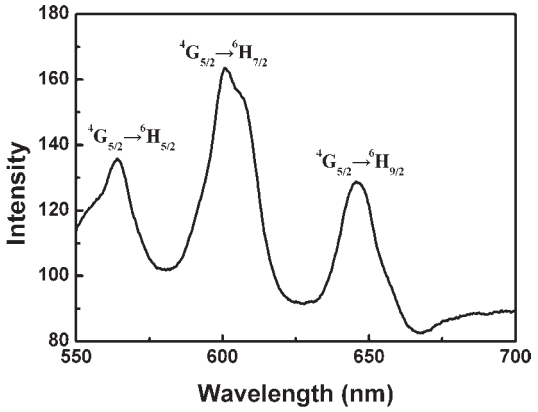

Figure 8. Solid-state emission spectrum of compound **5** at room temperature.

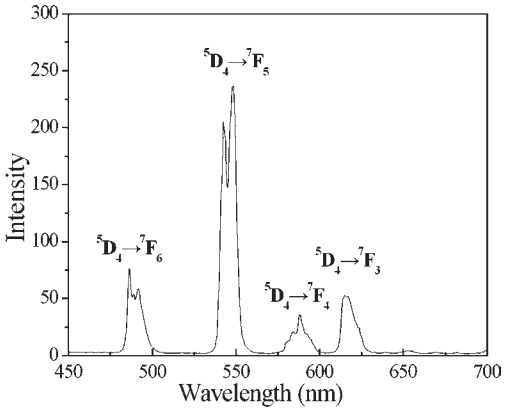

Figure 10. Solid-state emission spectrum of compound **8** at room temperature.

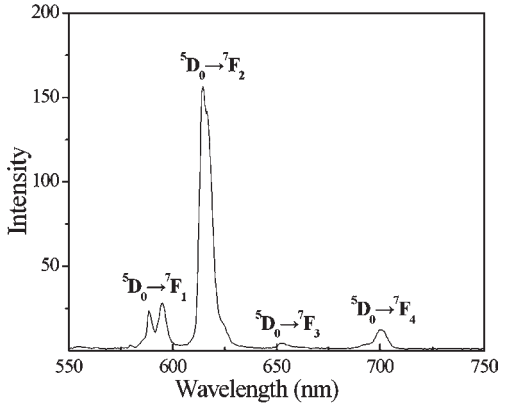

Figure 9. Solid-state emission spectrum of compound **6** at room temperature.

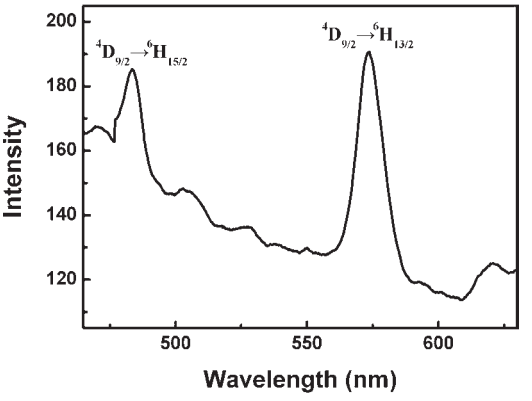

Figure 11. Solid-state emission spectrum of compound **9** at room temperature.

corresponds to a magnetic dipole transition, and the intensity of this emission for **6** is medium−strong. The most intense emission in the luminescent spectrum is the $^5D_0 \rightarrow {}^7F_2$ transition, which is the so-called hypersensitive transition and is responsible for the brilliant-red emission of compound **6**.[24] It is noted that the intensity of the hypersensitive transition $^5D_0 \rightarrow {}^7F_2$ is comparable to that of $^5D_0 \rightarrow {}^7F_1$. Since the former transition is electric dipole in nature, its intensity is strongly influenced by the crystal field while the latter transition is magnetic dipole in origin and less sensitive to its environment. Compound **8** exhibits four strong characteristic emission bands when excited at 378 nm (Figure 10). These emission bands are assigned to the $^5D_4 \rightarrow {}^7F_J$ (J = 3, 4, 5, and 6), $^5D_4 \rightarrow {}^7F_6$ (486 nm), $^5D_4 \rightarrow {}^7F_5$ (548 nm), $^5D_4 \rightarrow {}^7F_4$ (588 nm), and $^5D_4 \rightarrow {}^7F_3$ (615 nm) transitions.[25] Among these emission lines, the most striking green luminescence ($^5D_4 \rightarrow {}^7F_5$) for compound **8** is observed in the emission spectrum. Compound **9** is yellow luminescent in the solid state when excited at 352 nm. In the emission spectrum of compound **9** (Figure 11), two characteristic bands can be seen, which are attributed to transitions of 484 ($^4D_{9/2} \rightarrow {}^6H_{15/2}$) and 574 nm ($^4D_{9/2} \rightarrow {}^6H_{13/2}$).[9a] Compared with the emission spectra of the four compounds (**5**, **6**, **8**, and **9**), the transition intensity of compound **5** is the weakest. The low emission intensity for Sm^{3+} ions implies that the efficiency of energy transfer from ligands to metals is lower than that to Eu^{3+}, Tb^{3+}, and Dy^{3+}. Furthermore,

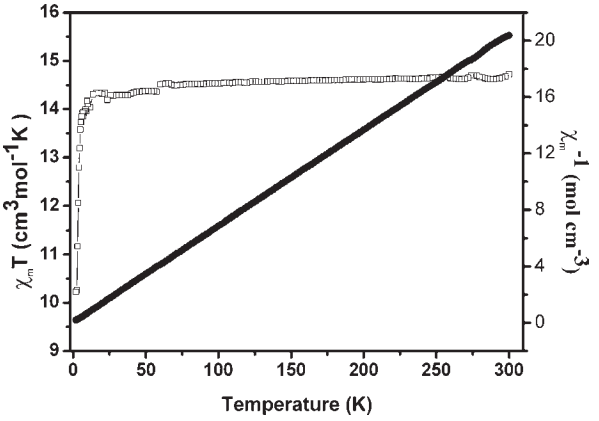

Figure 12. Thermal variations of $\chi_m T$ (□) and $1/\chi_m$ (●) for compound **7**.

the intensity of the four complexes based on the $hedpH_4$ ligand is completely weak, possibly due to the coordinated water molecules, which reduces the luminescent intensity of the rare earth ions,[26] and the energy transfer from the $hedpH_4$ ligand to lanthanide(III) ions is inefficient in the theory of energy transfer.[27]

Magnetic Property. The temperature dependence of the $\chi_m T$ product and inverse magnetic susceptibility ($1/\chi_m$) for

compound **7** at 1000 Oe in the temperature range 2−300 K are shown in Figure 12. The observed $\chi_m T$ value at 300 K of 14.74 cm^3 K mol^{-1} corresponds exactly to the expected value of 15.75 cm^3 K mol^{-1} for two uncoupled Gd^{III} ions ($S = 7/2$, $^8S_{7/2}$, and $g = 2$). It remains almost constant down to about 30 K, below which the $\chi_m T$ value decreases with decreasing temperature. The decline in $\chi_m T$ at low temperature can be attributed to antiferromagnetic exchange coupling between the magnetic centers across the O−P−O units. Since the O−P−O unit is not efficient in mediating magnetic exchange due to electron localization, the overall antiferromagnetic interaction in two Gd^{III} ions would be expected to be very weak. This is indeed the case. The inverse susceptibility plot as a function of temperature is linear above 2.0 K, following the Curie−Weiss law ($\chi_m^{-1} = 0.05743 + 0.06809T$) ($r = 0.99999$), with C = 14.69 cm^3 K mol^{-1} and Θ = −0.84 K, corresponding to about two S = 7/2 spin per formula. The decrease of the $\chi_m T$ value with decreasing temperature and negative Θ value suggest a weak antiferromagnetic interaction of Gd^{III} ions.[28]

CONCLUSION

Using the heptadentate ligand $hedpH_4$ and lanthanide chloride, 11 novel 3D chiral and achiral lanthanide diphosphonates with left- and right-handed helical chains have been synthesized under hydrothermal conditions and structurally characterized. Compounds **1**−**4** are isomorphous and feature a 3D framework formed by the interconnection of LnO_8 and CPO_3 polyhedra through phosphonate ligands. Compounds **5**−**11** are also isomorphous and exhibit some similar 3D network topologies with compounds **1**−**4**. The charge-compensating protonated NH_4^+ ions as templates located inside these channels with extensive hydrogen-bonding interactions play important roles to induce the 3D structure. The crystal water molecule with extensive hydrogen-bonding interactions, which change the molecular steric orientation of protonated NH_4^+, induce NH_4^+ as templates to form a chiral configuration. Thus, the steric orientation of protonated NH_4^+ is very important, which was adjusted by the crystal water molecule that induces different structural packing, steric orientation, and symmetry breaking. The phenomenon of the crystal water molecule to induce NH_4^+ as a template to form chiral configuration by extensive hydrogen-bonding interactions is still rare to this day. The results of our study indicate that by introduction of NH_4^+ ions as a template we can obtain chiral lanthanide diphosphonates with good crystals and induce chiral structure through a crystal water molecule with extensive hydrogen bonding. The luminescence properties of compounds **5**, **6**, **8**, and **9** and magnetic property of compound **7** have been studied. The Eu and Tb compounds exhibit strong luminescence in the red and green regions, respectively. The Gd compound exhibits a weak antiferromagnetic interaction between two Gd^{III} ions.

ASSOCIATED CONTENT

Supporting Information. X-ray crystallographic files in CIF format for compounds **1**−**11**, tables listing selected bond lengths and angles for compounds presented in this paper, XRD patterns of the experiments compared to those simulated from X-ray single-crystal data for compounds **1**−**11**, IR spectra of compounds **1**−**11**, and TGA curves of **1**−**11**. This material is available free of charge via the Internet at http://pubs.acs.org. CCDC 760609−760619 contain the supplementary crystallographic data for this paper. These data can be obtained free of charge www.ccdc.cam.ac.uk/conts/retrieving.html (or from the Cambridge Crystallographic Data Center, 12, Union Road, Cambridge CB21EZ, UK; fax: (+44) 1223−336−033; e-mail: deposit@ccdc.cam.ac.uk).

AUTHOR INFORMATION

Corresponding Author
*E-mail: szg188@163.com.

ACKNOWLEDGMENT

This work was supported by the National Natural Science Foundation of China (Grant No. 21071072).

REFERENCES

(1) (a) Maeda, K. *Microporous Mesoporous Mater.* **2004**, *73*, 47–55 and references therein. (b) Clearfield, A. *Curr. Opin. Solid State Mater. Sci.* **1996**, *1*, 268.(c) Clearfield, A. Metal phosphonate chemistry. In *Progress in Inorganic Chemistry*; Karlin, K. D., Ed.; John Wiley & Sons: New York, 1998; Vol. 47, pp 371−510 (and references therein). (d) Cheetham, A. K.; Férey, G.; Loiseau, T. *Angew. Chem., Int. Ed.* **1999**, *38*, 3268–3292. (e) Clearfield, A. *Dalton Trans.* **2008**, 6089–6102. (f) Hamada, A.; Braunstein, P. *Inorg. Chem.* **2009**, *48*, 1624–1637.

(2) (a) Fanucci, G. E.; Krzystek, J.; Meisel, M. W.; Brunel, L.-C.; Talham, D. R. *J. Am. Chem. Soc.* **1998**, *120*, 5469–5479. (b) Plabst, M.; McCusker, L. B.; Bein, T. *J. Am. Chem. Soc.* **2009**, *131*, 18112–18118. (c) Wharmby, M. T.; Mowat, J. P. S.; Thompson, S. P.; Wright, P. A. *J. Am. Chem. Soc.* **2011**, *133*, 1266–1269. (d) Feng, G.; Tanifum, E. A.; Adams, H.; Hengge, A. C.; Williams, N. H. *J. Am. Chem. Soc.* **2009**, *131*, 12771–12779.

(3) (a) Taylor, J. M.; Mah, R. K.; Moudrakovski, I. L.; Ratcliffe, C. I.; Vaidhyanathan, R.; Shimizu, G. K. H. *J. Am. Chem. Soc.* **2010**, *132*, 14055–14057. (b) Youngblood, W. J.; Lee, S.-H. A.; Kobayashi, Y.; Hernandez-Pagan, E. A.; Hoertz, P. G.; Moore, T. A.; Moore, A. L.; Gust, D.; Mallouk, T. E. *J. Am. Chem. Soc.* **2009**, *131*, 926–927. (c) Miller, S. R.; Pearce, G. M.; Wright, P. A.; Bonino, F.; Chavan, S.; Bordiga, S.; Margiolaki, I.; Guillou, N.; Férey, G.; Bourrelly, S.; Llewellyn, P. L. *J. Am. Chem. Soc.* **2008**, *130*, 15967–15981.

(4) Shimizu, G. K. H.; Vaidhyanathan, R.; Taylor, J. M. *Chem. Soc. Rev.* **2009**, *38*, 1430–1449.

(5) (a) Fu, R. B.; Xiang, S. C.; Zhang, H. S.; Zhang, J. J.; Wu, X. T. *Cryst. Growth Des.* **2005**, *5*, 1795–1799. (b) Burgomaster, P. D.; Aldous, A.; Liu, H.; O'Connor, C. J.; Zubieta, J. *Cryst. Growth Des.* **2010**, *10*, 2209–2218. (c) Hou, J. J.; Zhang, X. M. *Cryst. Growth Des.* **2006**, *6*, 1445–1452. (d) Guo, Y. Q.; Yang, B. P.; Song, J. L.; Mao, J. G. *Cryst. Growth Des.* **2008**, *8*, 600–605. (e) Chen, Z.; Zhou, Y.; Weng, L.; Zhao, D. *Cryst. Growth Des.* **2008**, *8*, 4045–4053. (f) Chen, S.; Huang, G.; Li, M.; Pan, L.; Yuan, Y.; Yuan, L. *Cryst. Growth Des.* **2008**, *8*, 2824–2833. (g) Ding, D. G.; Wu, B. L.; Fan, Y. T.; Hou, H. W. *Cryst. Growth Des.* **2009**, *9*, 508–516.

(6) (a) Yang, B. P.; Prosvirin, A. V.; Guo, Y. Q.; Mao, J. G. *Inorg. Chem.* **2008**, *47*, 1453–1459. (b) Ramaswamy, P.; Prabhu, R.; Natarajan, S. *Inorg. Chem.* **2010**, *49*, 7927–7934. (c) Feyand, M.; Näther, C.; Rothkirch, A.; Stock, N. *Inorg. Chem.* **2010**, *49*, 11158–11163. (d) Zhou, T. H.; Yi, F. Y.; Li, P. X.; Mao, J. G. *Inorg. Chem.* **2010**, *49*, 905–915. (e) Bauer, S.; Muller, H.; Bein, T.; Stock, N. *Inorg. Chem.* **2005**, *44*, 9464–9470.

(7) (a) Cao, D. K.; Xie, X. J.; Li, Y. Z.; Zheng, L. M. *Dalton Trans.* **2008**, *37*, 5008–5015. (b) Ma, K.; Xu, J.; Zhang, L.; Shi, J.; Zhang, D.; Zhu, Y.; Fan, Y.; Song, T. *New J. Chem.* **2009**, *33*, 886–892. (c) Guo, L. R.; Bao, S. S.; Li, Y. Z.; Zheng, L. M. *Chem. Commun.* **2009**, 2893–2895. (d) Wang, P. F.; Duan, Y.; Wang, T. W.; Li, Y. Z.; Zheng, L. M. *Dalton Trans.* **2010**, *39*, 10631–10636. (e) Li, J. T.; Cao, D. K.; Akutagawab, T.; Zheng, L. M. *Datlon Trans.* **2010**, *39*, 8606–8608.

(8) (a) Zhu, J.; Bu, X.; Feng, P.; Stucky, G. D. *J. Am. Chem. Soc.* **2000**, *122*, 11563–11564. (b) Zhang, X. *Eur. J. Inorg. Chem.* **2004**, 544–548. (c) Kubíček, V.; Kotek, J.; Hermann, P.; Lukeš, I. *Eur. J. Inorg. Chem.* **2007**, 333–344. (d) Du, Z. Y.; Sun, Y. H.; Xu, X.; Xu, G. H.; Xie, Y. R. *Eur. J. Inorg. Chem.* **2010**, 4865–4869.

(9) (a) Zhu, Y. Y.; Sun, Z. G.; Chen, H.; Zhang, J.; Zhao, Y.; Zhang, N.; Liu, L.; Lu, X.; W, W. N.; Tong, F. *Cryst. Growth Des.* **2009**, *9*, 3288–3234. (b) Liu, L.; Sun, Z. G.; Zhang, N.; Zhu, Y. Y.; Zhao, Y.; Lu, X.; Tong, F.; Wang, W. W.; Huang, C. Y. *Cryst. Growth Des.* **2010**, *10*, 406–413. (c) Zhu, Y. Y.; Sun, Z. G.; Tong, F.; Liu, Z. M.; Huang, C. Y.; Wang, W. N.; Jiao, C. Q.; Wang, C. L.; Li, C.; Chen, K. *Dalton Trans.* **2011**, *40*, 5584–5590. (d) Tong, F.; Sun, Z. G.; Chen, K.; Zhu, Y. Y.; Wang, W. N.; Jiao, C. Q.; Wang, C. L.; Li, C. *Dalton Trans.* **2011**, *40*, 5059–5065.

(10) (a) Adelani, P. O.; Oliver, A. G.; Albrecht-Schmitt, T. E. *Cryst. Growth Des.* **2011**, *11*, 1966–1973. (b) Armatas, N. G.; Allis, D. G.; Prosvirin, A.; Carnutu, G.; O'Connor, C. J.; Dunbar, K.; Zubieta, J. *Inorg. Chem.* **2008**, *47*, 832–854. (c) Barthelet, K.; Nogues, M.; Riou, D.; Férey, G. *Chem. Mater.* **2002**, *14*, 4910–4918. (d) Tan, H.; Chen, W.; Liu, D.; Li, Y.; Wang, E. *Dalton Trans.* **2010**, *39*, 1245–1249.

(11) (a) Ngo, H. L.; Lin, W. *J. Am. Chem. Soc.* **2002**, *124*, 14298–14299. (b) Evans, O. R.; Ngo, H. L.; Lin, W. *J. Am. Chem. Soc.* **2001**, *123*, 10395–10396. (c) Shi, X.; Zhu, G. S.; Qiu, S. L.; Huang, K. L.; Yu, J. H.; Xu, R. R. *Angew. Chem., Int. Ed.* **2004**, *43*, 6482–6485. (d) Yue, Q.; Yang, J.; Li, G. H.; Li, G. D.; Chen, J. S. *Inorg. Chem.* **2006**, *45*, 4431–4439. (e) Liu, X. G.; Bao, S. S.; Li, Y. Z.; Zheng, L. M. *Inorg. Chem.* **2008**, *47*, 5525–5527. (f) Liu, X. G.; Huang, J.; Bao, S. S.; Li, Y. Z.; Zheng, L. M. *Dalton Trans.* **2009**, *38*, 9837–9842.

(12) (a) Dong, D. P.; Sun, Z. G.; Tong, F.; Zhu, Y. Y.; Chen, K.; Jiao, C. Q.; Wang, C. L.; Li, C.; Wang, W. N. *CrystEngComm.* **2011**, *13*, 3317–3320. (b) Tan, H. Q.; Chen, W. L.; Liu, D.; Li, Y. G.; Wang, E. B. *CrystEngComm.* **2010**, *12*, 4017–4019. (c) Hou, S. Z.; Cao, D. K.; Li, Y. Z.; Zheng, L. M. *Inorg. Chem.* **2008**, *47*, 10211–10213.

(13) (a) Tong, X. L.; Hu, T. L.; Zhao, J. P.; Wang, Y. K.; Zhang, H.; Bu, X. H. *Chem. Commun.* **2010**, *46*, 8543–8545. (b) Li, J. R.; Tao, Y.; Yu, Q.; Bu, X. H.; Sakamoto, H.; Kitagawa, S. *Chem.—Eur. J.* **2008**, *14*, 2771–2776. (c) Liu, F. C.; Zeng, Y. F.; Zhao, J. P.; Hu, B. W.; Sañudo, E. C.; Ribas, J.; Bu, X. H. *Inorg. Chem.* **2007**, *46*, 7698–7700. (d) Du, M.; Bu, X. H.; Guo, Y. M.; Ribas, J.; Diaz, C. *Chem. Commun.* **2002**, 2550–2551. (e) Bu, X. H.; Chen, W.; Du, M.; Biradha, K.; Wang, W. Z.; Zhang, R. H. *Inorg. Chem.* **2002**, *41*, 437–439.

(14) (a) Morris, R. E.; Bu, X. *Nat. Chem.* **2010**, *2*, 353–361. (b) Zhang, J.; Chen, S.; Nieto, R. A.; Wu, T.; Feng, P.; Bu, X. *Angew. Chem., Int. Ed.* **2010**, *49*, 1267–1270. (c) Zhang, J.; Bu, X. *Angew. Chem., Int. Ed.* **2007**, *46*, 6115–6118. (d) Chen, X. D.; Du, M.; Mak, T. C. W. *Chem. Commun.* **2005**, 4417–4419. (e) Pérez-García, L.; Amabilino, D. B. *Chem. Soc. Rev.* **2002**, *31*, 342–356. (f) Biradha, K.; Seward, C.; Zaworotko, M. J. *Angew. Chem., Int. Ed.* **1999**, *38*, 492.

(15) (a) Zheng, L. M.; Song, H. H.; Xin, X. Q. *Comments Inorg. Chem.* **2000**, *22*, 129–149. (b) Rocha, J.; Paz, F. A. A.; Shi, F. N.; Ferreira, R. A. S.; Trindade, T.; Carlos, L. D. *Eur. J. Inorg. Chem.* **2009**, 4931–4945. (c) Rocha, J.; Shi, F. N.; Paz, F. A. A.; Mafra, L.; Sardo, M.; Cunha-Silva, L.; Chisholm, J.; Ribeiro-Claro, P.; Trindade, T. *Chem.—Eur. J.* **2010**, *16*, 7741–7749.

(16) (a) Yin, P.; Zheng, L. M.; Gao, S.; Xin, X. Q. *Chem. Commun.* **2001**, 2346–2347. (b) Yin, P.; Gao, S.; Zheng, L. M.; Xin, X. Q. *Chem. Mater.* **2003**, *15*, 3233–3236. (c) Zheng, L. M.; Gao, S.; Yin, P.; Xin, X. Q. *Inorg. Chem.* **2004**, *43*, 2151–2156. (d) Liu, B.; Li, Y. Z.; Zheng, L. M. *Inorg. Chem.* **2005**, *44*, 6921–6923. (e) Liu, B.; Yin, P.; Yi, X. Y.; Gao, S.; Zheng, L. M. *Inorg. Chem.* **2006**, *45*, 4205–4213.

(17) (a) Shi, F. N.; Cunha-Silva, L.; Ferreira, R. A. S.; Mafra, L.; Trindade, T.; Carlos, L. D.; Paz, F. A. A.; Rocha, J. *J. Am. Chem. Soc.* **2008**, *130*, 150–167. (b) Liu, F. Y.; Roces, L.; Sa Ferreira, R. A.; García-Granda, S.; García, J. R.; Carlos, L. D.; Rocha, J. *J. Mater. Chem.* **2007**, *17*, 3696–3701.

(18) Chen, H.; Li, J.; Sun, Z. G.; Zhu, Y. Y.; Zhang, J.; Zhao, Y.; Zhang, N.; Lu, X.; Liu, L. *J. Coord. Chem.* **2009**, *62*, 294–301.

(19) (a) Zhu, Y.; Sun, Z.; Zhao, Y.; Zhang, J.; Lu, X.; Zhang, N.; Liu, L.; Tong, F. *New J. Chem.* **2009**, *33*, 119–124. (c) Zhang, N.; Sun, Z.; Zhu, Y.; Zhang, J.; Liu, L.; Huang, C.; Lu, X.; Wang, W.; Tong, F. *New J. Chem.* **2010**, *34*, 2429–2435.

(20) (a) Song, J. L.; Yi, F. Y.; Mao, J. G. *Cryst. Growth Des.* **2009**, *9*, 3273–3277. (b) Hu, X.; Dou, W.; Xu, C.; Tang, X.; Zheng, J.; Liu, W. *Dalton Trans.* **2011**, *40*, 3412–3418.

(21) Shannon, R. D. *Acta Crystallogr.* **1976**, *A32*, 751–767.

(22) (a) Cabeza, A.; Ouyang, X.; Sharma, C. V. K.; Aranda, M. A. G.; Bruque, S.; Clearfield, A. *Inorg. Chem.* **2002**, *41*, 2325–2333. (b) Sun, Z. M.; Mao, J. G.; Yang, B. P.; Ying, S. M. *Solid State Sci.* **2004**, *6*, 295–300.

(23) Song, J. L.; Mao, J. G. *Chem.—Eur. J.* **2005**, *11*, 1417–1424.

(24) (a) de Bettencourt-Dias, A. *Inorg. Chem.* **2005**, *44*, 2734–2741. (b) Law, G. L.; Wong, K. L.; Zhou, X.; Wong, W. T.; Tanner, P. A. *Inorg. Chem.* **2005**, *44*, 4142–4144.

(25) (a) Tang, S. F.; Song, J. L.; Li, X. L.; Mao, J. G. *Cryst. Growth. Des.* **2006**, *6*, 2322–2326. (b) Bao, S. S.; Ma, L. F.; Wang, Y.; Fang, L.; Zhu, C. J.; Li, Y. Z.; Zheng, L. M. *Chem.—Eur. J.* **2007**, *13*, 2333–2343.

(26) Xia, J.; Zhao, B.; Wang, H.-S.; Shi, W.; Ma, Y.; Song, H.-B.; Cheng, P.; Liao, D.-Z.; Yan, S.-P. *Inorg. Chem.* **2007**, *46*, 3450–3458.

(27) Dexter, D. L. *J. Chem. Phys.* **1953**, *21*, 836–839.

(28) Ma, Y. S.; Li, H.; Wang, J. J.; Bao, S. S.; Cao, R.; Li, Y. Z.; Ma, J.; Zheng, L. M. *Chem.—Eur. J.* **2007**, *13*, 4759–4769.